Published in final edited form as:
J Proteome Res. 2009 October ; 8(10): 4823. doi:10.1021/pr900561g.

ATP-Sensitive K^+ Channel Knockout Induces Cardiac Proteome Remodeling Predictive of Heart Disease Susceptibility

D. Kent Arrell, **Jelena Zlatkovic**, **Garvan C. Kane**, **Satsuki Yamada**, and **Andre Terzic***
Marriott Heart Disease Research Program, Division of Cardiovascular Diseases, Departments of Medicine, Molecular Pharmacology and Experimental Therapeutics, and Medical Genetics, Mayo Clinic, Rochester, Minnesota 55905

Abstract

Forecasting disease susceptibility requires detection of maladaptive signatures prior to onset of overt symptoms. A case-in-point are cardiac ATP-sensitive K^+ (K_{ATP}) channelopathies, for which the substrate underlying disease vulnerability remains to be identified. Resolving molecular pathobiology, even for single genetic defects, mandates a systems platform to reliably diagnose disease predisposition. High-throughput proteomic analysis was here integrated with network biology to decode consequences of Kir6.2 K_{ATP} channel pore deletion. Differential two-dimensional gel electrophoresis reproducibly resolved > 800 protein species from hearts of asymptomatic wild-type and Kir6.2-knockout counterparts. K_{ATP} channel ablation remodeled the cardiac proteome, significantly altering 71 protein spots, from which 102 unique identities were assigned following hybrid linear ion trap quadrupole-Orbitrap tandem mass spectrometry. Ontological annotation stratified the K_{ATP} channel-dependent protein cohort into a predominant bioenergetic module (63 resolved identities), with additional focused sets representing signaling molecules (6), oxidoreductases (8), chaperones (6), and proteins involved in catabolism (6), cytostructure (8), and transcription and translation (5). Protein interaction mapping, in conjunction with expression level changes, localized a K_{ATP} channel-associated subproteome within a nonstochastic scale-free network. Global assessment of the K_{ATP} channel deficient environment verified the primary impact on metabolic pathways and revealed overrepresentation of markers associated with cardiovascular disease. Experimental imposition of graded stress precipitated exaggerated structural and functional myocardial defects in the Kir6.2-knockout, decreasing survivorship and validating the forecast of disease susceptibility. Proteomic cartography thus provides an integral view of molecular remodeling in the heart induced by K_{ATP} channel deletion, establishing a systems approach that predicts outcome at a presymptomatic stage.

Keywords

channelopathy; individualized medicine; K_{ATP} channel; KCNJ11; Kir6.2; network; predictive medicine; proteomics; systems biology

Introduction

The tenets of predictive medicine offer a paradigm shift from reactive traditional approaches to manage overt heart disease toward proactive interventions tailored to prevent or mitigate

* To whom correspondence should be addressed. Dr. Andre Terzic, Mayo Clinic, Stabile 5, 200 First Street SW, Rochester, MN 55905. terzic.andre@mayo.edu. Fax: + 1-507-266-9936.

Supporting Information Available: Supplementary Table 1, which contains acquired mass spectral data for all identified proteins. This material is available free of charge via the Internet at http://pubs.acs.org.

disease manifestation. Predictive medicine is enabled by mechanistic insights extracted from divergence of disease-prone cellular networks from their normal counterparts.[1,2] Decoding inherent maladaptive signatures prior to symptom onset would guide rational forecasting of individual disease susceptibility.[3,4] To date, however, subclinical molecular profiles predictive of heart disease remain only partially characterized, limiting realization of anticipatory solutions.

To this end, resolving cardioprotective processes and their underlying systems organization is a critical step in comprehending cardiac homeostasis in health and disease. A case-in-point is the metabolism-gated ATP-sensitive K^+ (K_{ATP}) channel, a prototypic biosensor that enables high fidelity readout of metabolic distress signals.[5–8] Unique among ion channels, this checkpoint performs a rheostat-like operation adjusting membrane potential-dependent functions to match energetic demands of the working heart.[9–12] Abundant in the myocardial sarcolemma, K_{ATP} channel complexes form through assembly of the *KCNJ11*-encoded Kir6.2 pore with the regulatory ATP-binding cassette sulfonylurea receptor subunits.[13–16] K_{ATP} channel dysfunction compromises vital homeostatic functions leading to life-threatening conditions.[17–20] While K_{ATP} channelopathies are increasingly implicated in human cardiac pathologies,[21–23] the molecular consequences of channel deficiency that predispose to disease vulnerability have yet to be dissected.

Systems platforms offer a means of reliably integrating pathobiologic complexity to predict disease predisposition.[24–27] In this regard, proteomics methods provide a high-throughput, unbiased approach for large-scale identification of proteins responsible for (patho) physiological processes. Herein, we demonstrate extensive protein alterations in response to K_{ATP} channel ablation, which collectively comprise an integrated, scale-free network, with an overarching function of energy metabolism and overrepresentation of markers associated with cardiovascular disease. Subsequent experimental validation of K_{ATP} channel knockout cardiomyopathic predisposition underscores the utility of a systems-based approach to anticipate outcome from a presymptomatic profile.

Materials and Methods

K_{ATP} Channel Knockout and Cardiac Tissue Fractionation

K_{ATP} channel-deficient mice (Kir6.2-KO) were generated by targeted disruption of *KCNJ11*, encoding the pore-forming Kir6.2 channel subunit of myocardial K_{ATP} channels, and backcrossed for 5 generations to a C57BL/6 background.[28] Animal protocols followed NIH guidelines, and received Mayo Clinic Institutional Animal Care and Use Committee approval. Cardiac function of adult age-matched wild-type (WT) and Kir6.2-KO male mice was compared by M-mode echocardiography, a standard measure of heart contractility.[19,21] Animals were weighed, anesthetized with isoflurane, and hearts were removed and weighed with the left ventricle including septum excised and snap-frozen in liquid N_2. Cytosolic tissue extracts were prepared by homogenization at 4 °C in extraction buffer, consisting of (in mM) HEPES 25 (pH 7.4), PMSF 0.25, DTT 50, 1.25 μM pepstatin A, Mini-Complete protease inhibitor cocktail (Roche Applied Science), and 1% phosphatase inhibitor cocktails 1 and 2 (Sigma). Homogenized samples were centrifuged (16 000*g*) at 4 °C for 10 min, and supernatant protein content quantified in triplicate by microassay procedure.[29–31]

Two-Dimensional Gel Electrophoresis and Image Analysis

Protein extracts (100 μg) were resolved by immobilized pH gradient (IPG) 2-DE following addition to isoelectric focusing (IEF) rehydration buffer (7 M urea, 2 M thiourea, 2% w/v CHAPS, 50 mM DTT, 1× Bio-Rad pH 3–10 ampholytes). IPG Ready Strips (pH 3–10 170 mm, Bio-Rad) were actively rehydrated, followed by IEF using a series of voltage ramping

steps to a total of 60 kVh.[32] Focused IPG strips were reduced in equilibration buffer (50 mM Tris-HCl, pH 8.8, 6 M urea, 30% v/v glycerol, 2% w/v SDS) supplemented with 10 mg/mL DTT, followed by alkylation in equilibration buffer containing 25 mg/mL iodoacetamide. Proteins were resolved orthogonally by 12.5% SDS-PAGE in a Bio-Rad Protean II XL system. [33] Resolved gels were silver-stained and digitized for image analysis conducted with Bio-Rad PDQuest v.7.4.0.[32–34] Gel images were normalized by densitometric quantitation of valid spots for fold-change determination. For proteins identified in more than one spot, the sum of values for all spots was used to determine a weighted average.[32]

Nanoelectrospray Linear Ion Trap Tandem Mass Spectrometry

Altered protein species were isolated, destained, and prepared for LC-MS/MS.[32–34] Peptides were reconstituted in 0.15% formic acid, 0.05% TFA, and trap injected onto a 75 μm × 5 cm ProteoPep C18 PicoFrit nanoflow column (New Objective). Chromatography was performed using an Eksigent nanoHPLC system (MDS Sciex) coupled to an LTQ-Orbitrap mass spectrometer (Thermo Fisher Scientific). Continuous scanning for eluting peptide ions was carried out between 375–1600 *m*/*z*, automatically switching to MS/MS CID mode on ions exceeding an intensity of 8000. Raw MS/MS spectral data were converted to .dta files using Bioworks 3.2 (Thermo Fisher Scientific), and merged files correlated to theoretical tryptic fragments in Swiss-Prot (v.53.0 comprised of 269 293 sequences) using Mascot v.2.2.[32] Searches were conducted on mammalian sequences (53 539 entries), with up to 2 missed cleavages, mass tolerances of ±0.01 Da for precursor ions (with ^{13}C peak correction) and ±0.6 Da for product ions, and allowance for protein N-terminal acetylation, methionine oxidation or cysteine carbamidomethylation. Protein identities were confirmed by matching multiple peptide spectra at $P < 0.05$, with proteins accepted at $P < 0.01$.[26] Proteins identified by a single peptide were thus subject to a higher stringency level ($P < 0.01$), and were also confirmed by manual spectrum inspection, with detected fragment ions from the MS/MS spectrum required to be above baseline noise, have demonstrable continuity in b- or y-ion series, and proline residues yielding intense y-ions.[35] Positive matches to nonmouse species lacking Swiss-Prot mouse homologues were screened against the TrEMBL database to confirm a match to a mouse protein (indexed 2007–01–23, comprising 3 633 676 sequences). Protein assignments were further validated by congruence of observed versus predicted p*I*/M_r, using the ExPASy p*I*/M_r tool (us.expasy.org/tools/pi_tool.html), taking into consideration protein processing, known post-translational modifications, and predicted mitochondrial localization and signal peptide cleavage sites as determined using the established algorithm TargetP 1.1.[36]

Protein Interaction Network Analysis

Identified proteins, with their fold change ratios, were submitted as focus proteins for network analysis using Ingenuity Pathways Analysis (IPA, Ingenuity Systems) to predict a composite outcome through connection of functional subnetworks.[32,33] The composite was mapped using the network visualization algorithm Cytoscape 2.5.1,[37] with network topology assessed using Network Analyzer.[38] Node degree (k), the number of node connections, and node degree distribution (P[k]), the probability that a node has k links, where P[k] = X[k]/n, when X[k] is the number of nodes with degree k and n equals total nodes were used to define network architecture.[32] P[*k] versus k* discriminates between random and scale-free topographies,[39] defined by normal and power law distributions, respectively. The Anderson-Darling normality test[40] was used to rule out a normal distribution, so P[k] versus k was calculated as a power law relationship using a cumulative distribution function[41] to determine γ in the power law distribution ($P[k] \sim k^{-\gamma}$), using eq 1:

$$\gamma = 1 + n\left[\sum_{i=1}^{n} \ln \frac{x_i}{x_{\min}}\right]^{-1} \quad (1)$$

where γ is the power law exponent, n is the number of network nodes, x_i is the node degree, and $x_{\min}$ is the minimum node degree within the network, with statistical error σ[41] for eq 1 defined by eq 2:

$$\sigma = \sqrt{n}\left[\sum_{i=1}^{n} \ln \frac{x_i}{x_{\min}}\right]^{-1} = \frac{\gamma - 1}{\sqrt{n}} \quad (2)$$

Interrogation of the composite network was carried out with the Cytoscape module BiNGO 2.0 (Bioinformatic Network Gene Ontology), to assess Gene Ontology (GO) biological process enrichment,[42] providing an unbiased bioinformatic approach to interpret functional interdependencies within the composite network. IPA was also used to identify prioritized physiological or pathophysiological categories with connections to proteins comprising the resolved interaction network. Individual categories are considered for overrepresentation by IPA on the basis of statistical analysis of their proportional occurrence within the network relative to their overall occurrence in the entire proteome.

Imposition of Cardiac Stress

Mild, moderate or severe stress load was imposed, respectively, by aquatic endurance training,[43] volume overload induced hypertension,[19] and transverse aortic banding induced pressure overload[21] in adult age and sex-matched WT and Kir6.2-KO mice. In endurance training, collective swimming was carried out for 90 min, twice daily, over 28 days.[43] In volume overload, following unilateral nephrectomy, mineralocorticoid-hypertension was induced by 21-day release of a subcutaneous 50 mg deoxycorticosterone acetate pellet (Innovative Research of America) with 1% NaCl, 0.2% KCl drinking water supplementation.[19] In pressure overload, thoracic aortae were uniformly constricted to the diameter of a 27-gauge needle.[21] Left ventricular fractional shortening (FS) was calculated by M-mode echocardiography as a standard parameter of heart contractility, and left ventricle mass was measured to evaluate cardiomegaly, as previously described.[19,21,43]

Statistical Analysis

Unless otherwise indicated, comparison between groups was performed using a standard *t*-test of variables with 95% confidence intervals, and data expressed as mean ± SE. For BiNGO, a hypergeometric test with Benjamini and Hochberg false discovery rate correction was used to assess the protein network for significant overrepresentation of GO biological processes. Kaplan–Meier analysis with logrank testing was applied for survival analysis, with $P < 0.05$ predetermined.[44]

Results

Kir6.2 Ablation Transforms the Cardiac Proteome

Targeted disruption of *KCNJ11* generates Kir6.2-deficient mice that lack functional K_{ATP} channels in ventricular myocytes.[45] Stress-free K_{ATP} channel knockout (Kir6.2-KO) animals did not display apparent differences in cardiac function or gross heart morphology when compared to age- and sex-matched wild-type (WT) counterparts (Figure 1A). To assess the

potential spectrum of molecular consequences precipitated by K_{ATP} channel deficiency, the left ventricle of WT ($n = 4$) and Kir6.2-KO ($n = 4$) were subjected to comparative proteomic analysis. Separation of cytoplasmic tissue extracts by broad pH range 2-DE resolved >800 unique protein species (Figure 1B), with high gel-to-gel reproducibility (Figure 1C). Densitometric quantification of relative spot intensities as exemplified for spot 58 (Figure 1D) revealed that 71 of 804 (8.8%) protein species were significantly altered by Kir6.2 deletion ($P < 0.05$), a third of which increased while two-thirds decreased (Figure 1E). Thus, ablation of *KCNJ11* transforms the ventricular protein expression pattern unmasking a K_{ATP} channel-dependent cardiac subproteome.

Cartography of Kir6.2-Knockout Proteome

To determine the identity of protein alterations induced by Kir6.2 deletion, a discriminatory analysis of cytoplasmic subproteomes was carried out by linear ion trap quadrupole (LTQ) Orbitrap MS/MS of in-gel tryptic digests. Using a stringent cutoff ($P < 0.01$) for protein identity, assignments were obtained for 62 of the 71 altered protein species, matching derived spectra to multiple unique peptides *per* protein or, for proteins identified by a single peptide match, by subsequent manual inspection of the MS/MS spectrum (Supplementary Table 1, Supporting Information). Collectively, a total of 102 intracellular protein assignments were obtained (Figure 2 and 3). Ontological annotation stratified the K_{ATP} channel-dependent protein cohort into a predominant bioenergetic module (63/102 proteins), including mitochondrial proteins, primarily dehydrogenases and transferases involved in the tricarboxylic acid cycle or fatty acid β-oxidation pathway, cytoplasmic proteins primarily functioning within the glycolytic pathway, as well as a variety of enzymes contributing to amino acid or nucleic acid metabolism (Figure 2). Multiple changes (39/102 proteins) were also detected in nonmetabolic functional classes, comprising signaling molecules, oxidoreductases and chaperones, as well as proteins involved in catabolism, cytostructure, and transcription/translation (Figure 3). Thus, resolution of the identity of specific proteins contributing to the cardiac K_{ATP} channel subproteome revealed a broad spectrum of compromised cellular processes.

K_{ATP} Channel-Dependent Subproteome Network Topography and Ontological Annotation

Network analysis was carried out to obtain a collective understanding of processes associated with the remodeled proteome in the setting of K_{ATP} channel deficiency. Protein–protein interaction mapping clustered K_{ATP} channel-dependent proteins into an organized network comprised of 221 nodes linked by 928 edges. Ontological assessment of individual proteins validated the primary functional impact on metabolic pathways observed with the proteomic data, with all network elements accounted for by identical classifications (Figure 4A and B). The nonrandomness of network topology was confirmed by derivation of network degree distribution, the interrelationship between the network variables node degree (k) and node degree distribution [$P(k)$]. After ruling out a random distribution using the Anderson-Darling normality test ($P = 1.52 \times 10^{-9}$), a cumulative distribution function was applied to define a nonstochastic scale-free architecture, following a power law distribution where $P(k) \sim k^{-\gamma}$, with $\gamma = 1.653 \pm 0.044$ (Figure 4C), which falls within parameters characteristic of biological networks.[39]

Network assessment with BiNGO to identify network node GO biological process enrichment verified the overarching prevalence of bioenergetic components, as 87% of unique network protein nodes were linked to metabolism, as were all 55 biological processes overrepresented ($P < 0.001$) within the full ontological spectrum of 962 potential processes associated with the derived K_{ATP} channel-dependent network (Figure 5). Indeed, biological processes linked to glycolysis, fatty acid metabolism, the tricarboxylic acid cycle, and protein catabolism demonstrated the greatest extent of statistical overrepresentation. Dissection of the composite

network into discrete functional subnetworks further corroborated the massive contribution to bioenergetics, as amino acid metabolism, carbohydrate metabolism, and small molecule biochemistry were designated by Ingenuity Pathways Analysis as top functions associated with the most prominent subnetwork, comprising 24 of the 102 focus proteins, while carbohydrate metabolism, amino acid metabolism, and lipid metabolism were top functions for the second most prominent subnetwork, containing 18 focus proteins. Thus, the network encompassing the resolved K_{ATP} channel-dependent subproteome organizes into a *bona fide* biological system with an overwhelming bioenergetic ontological linkage to metabolic and metabolism related processes.

Forecast of Disease Predisposition Validated through Stress Imposition

The subproteome and associated network neighborhood database that underlie Kir6.2 deficiency provided a systems framework to screen for putative pathophysiological patterns arising from proteome remodeling. Collective bioinformatic interrogation of the K_{ATP} channel-dependent subproteome demonstrated an overrepresentation for the “cardiovascular disease” category predicting, *in silico*, heart disease susceptibility, a pattern reiterated and accentuated in the broader network interactome context (Figure 6A). To validate this prediction *in vivo*, WT and Kir6.2-KO cohorts were subjected to graded levels of imposed cardiac stress. Whereas no difference was evident prior to stress, with progressively greater stress challenge the absence of K_{ATP} channels was associated with aggravated increases in left ventricular mass and decreases in fractional shortening (Figure 6B and C). Ultimately, proteomic remodeling in response to Kir6.2 deletion precipitated a highly maladaptative cardiac stress response with decreasing survival arising from progressively increased stress (Figure 6D). In contrast, WT exhibited significant protection when subject to mild (0% mortality, $n = 18$), moderate (3%, $n = 24$) or severe stress (44%, $n = 28$) as compared to Kir6.2-KO counterparts - mild (21%, $n = 18$), moderate (45%, $n = 24$), severe (74%, $n = 108$, all $P < 0.01$ versus WT). Thus, while the K_{ATP} channel knockout does not display an overt cardiac disease phenotype in the absence of stress, proteomic remodeling in response to Kir6.2 deletion predisposes to aggravated outcome, establishing a molecular substrate for maladaptive response to stress that leads to increased morbidity and mortality in the setting of K_{ATP} channel deficit.

Discussion

This study establishes a previously unrecognized physiological role for K_{ATP} channels in supporting a broad subproteome vital to the well-being of the ventricular mammalian myocardium. Systems analysis of the cardiac subproteome remodeled in response to ablation of the K_{ATP} channel pore extracted a subclinical signature predicting susceptibility to cardiovascular disease at an otherwise asymptomatic state. By decoding molecular profiles predictive of disease manifestation, the present study offers a paradigm toward realizing the prospect of anticipatory medicine prior to symptom onset.

Traditionally, K_{ATP} channels have been associated with protection of the myocardium under stress.[8,17,18,46] Despite their discovery nearly three decades ago within the cardiac sarcolemma where they were found to be particularly abundant, understanding of K_{ATP} channel contributions has been limited to conditions of ischemic and more recently nonischemic challenge.[5,19,21,47,48] Their role, however, in the stress-free heart has remained largely an enigma.[49] The present demonstration that K_{ATP} channel deficiency, produced by ablation of the *KCNJ11*-encoding Kir6.2 pore, alters nearly 9% of all detected protein species within left ventricular extracts offers the first definitive evidence for a homeostatic requirement of K_{ATP} channels in ensuring stability of the normal cardiac proteome.

While cardiac K_{ATP} channels have been previously implicated in individual energy metabolism pathways,[50–54] herein disruption of channel biogenesis combined with high-throughput

proteomic cartography diagnosed extensive changes across a spectrum of metabolic processes, involving over 100 unique identities. Over 60% of the altered subproteome comprised enzymes implicated in mitochondrial metabolism via the tricarboxylic acid cycle and fatty acid β-oxidation, cytoplasmic metabolism primarily involving glycolysis, as well as contributors to both amino acid and nucleic acid metabolism. Among this broad spectrum of energetic molecules are proteins with established links to the cardiac K_{ATP} channel, including the glycolytic enzymes triosephosphate isomerase, pyruvate kinase, and glyceraldehyde-3-phosphate dehydrogenase,[52,53] the fatty acid biosynthesis enzyme long chain acyl-CoA dehydrogenase,[54] and contributors to cardiac energy shuttling, including creatine kinase isoforms and lactate dehydrogenase.[51,55,56] Beyond metabolism-centric protein partners, discrete clusters of signaling proteins, oxidoreductases, chaperones, catabolic proteins, and proteins supporting cytostructure, transcription and translation were also affected by disruption of K_{ATP} channel function. This study thereby demonstrates, under normal cellular physiological conditions, the identity of multiple molecular components constituting a robust K_{ATP} channel-dependent cardiac subproteome.

Charting protein–protein relationships authenticated the primary impact on metabolic pathways, and encompassed a wide influence of the K_{ATP} channel upon a 221 node network neighborhood. The resolved interactome fulfilled criteria of nonstochastic topography typical of authentic biological networks, which confers the capability of readily adopting optimal functional states.[39,57] Unbiased gene ontology-based network interrogation further extended the significance of the underlying K_{ATP} channel-dependent infrastructure, revealing bioenergetic ontological linkage of nearly 90% of network nodes to metabolism and metabolism-related processes. This iterative process of proteomic cartography and functional ontology thus details the K_{ATP} channel network as a biologically relevant, nonrandom, protein assembly.

Networks arising from established protein interactions provide a means for defining phenotypic outcome following perturbation.[58] In this study, removal of K_{ATP} channels corrupted the baseline proteome which translated into a prioritized susceptibility to “cardiovascular disease” within not only the remodeled subproteome but also the resultant interactome. There are, however, diverse examples of cardiac dysfunction whereby associated proteomic remodeling is either absent prior to symptom manifestation[59] or detectable but not extensive until disease onset,[60] suggesting the critical nature of K_{ATP} channels in endowing stress tolerance.

The bioinformatic forecast was directly validated through prospective exposure of the K_{ATP} channel knockout to increasing stress load, which led to progressive worsening of cardiac function, structure and, ultimately, diminished survival relative to the equivalently stressed wild-type. The observed stress intolerance is consistent with a fundamental protective role for K_{ATP} channels enabled through coordinated interactions with metabolic partners integrating ion homeostasis with energetic demands of the cell.[55,56,61] In fact, the pronounced metabolic remodeling in presymptomatic K_{ATP} channel knockouts, in concert with the inability to precondition the Kir6.2-KO against subsequent injury,[62] is in line with findings establishing extensive proteomic changes in response to distinct pharmacological agents[29] or hemodynamic stress[26] known to interact with[63–65] or involve[19] the cardioprotective K_{ATP} channel. A distinct example of change deciphered in the K_{ATP} channel deficient milieu is the downregulation of aldehyde dehydrogenase-2, recently implicated in cardiac protection against damage.[66,67] More broadly, metabolic remodeling ensuing from gene deletion of distinct cardioprotective molecules compromises the ability of the heart to match energy production with utilization, precipitating maladaptation to stress.[68–70] As heart muscle requires great dynamic flexibility to maintain cardiac performance in the face of continuous energetic demands in both health and disease,[71–73] acquired or, as shown here, congenital inability to adequately maintain metabolic integrity would preclude the adaptive flexibility required for cardioprotection.

The cardiac K_{ATP} channel has previously been established as a rheostat-like protein complex that matches cellular metabolic supply with demand in response to disease. Based on an unbiased systems biology approach, the present study establishes a critical, previously unrecognized, role for K_{ATP} channels in the stability of the normal cardiac proteome such that the heart can adequately respond to stress. Monogenic deletion of the *KCNJ11*-encoded Kir6.2 channel pore precipitated complex proteomic remodeling of a broad and interrelated K_{ATP} channel-dependent infrastructure within heart muscle. Beyond proteins with previously established links to the K_{ATP} channel, bioinformatic interrogation of the affected K_{ATP} channel subnetwork unmasked extensive metabolic restructuring associated with overrepresentation of "cardiovascular disease" markers. Validated experimentally by the differential response of the K_{ATP} channel knockout to graded stress, this approach to detect, identify and forecast disease-prone networks offers the opportunity to elicit a paradigm shift away from traditional post-onset disease management and toward subclinical detection, thus enabling earlier, presymptomatic intervention.

Supplementary Material

Refer to Web version on PubMed Central for supplementary material.

Acknowledgments

We thank Jonathan Nesbitt for surgical expertise and the Mayo Proteomics Research Center staff, particularly Benjamin Madden, Kenneth Johnson, Christopher Mason and Roman Zenka, for expert guidance in mass spectrometry and bioinformatic analysis. Support was provided by the National Institutes of Health, Marriott Heart Disease Research Program, and Mayo Clinic. D.K.A. is the recipient of a Marriott Individualized Medicine Career Development Award. J.Z. holds a Mayo Graduate School fellowship. S.Y. is the recipient of an American Society for Clinical Pharmacology and Therapeutics Young Investigator Award. A.T. holds the Marriott Family Professorship in Cardiovascular Research at Mayo Clinic.

References

1. Hood L, Heath JR, Phelps ME, Lin B. Systems biology and new technologies enable predictive and preventative medicine. Science 2004;306:640–3. [PubMed: 15499008]
2. Weston AD, Hood L. Systems biology, proteomics, and the future of health care: toward predictive, preventative, and personalized medicine. J Proteome Res 2004;3:179–96. [PubMed: 15113093]
3. Bell J. Predicting disease using genomics. Nature 2004;429:453–6. [PubMed: 15164070]
4. Waldman SA, Terzic A. Therapeutic targeting: a crucible for individualized medicine. Clin Pharmacol Ther 2008;83:651–4. [PubMed: 18425084]
5. Alekseev AE, Hodgson DM, Karger AB, Park S, Zingman LV, Terzic A. ATP-sensitive K^+ channel channel/enzyme multimer: Metabolic gating in the heart. J Mol Cell Cardiol 2005;38:895–905. [PubMed: 15910874]
6. Ashcroft FM. ATP-sensitive potassium channelopathies: Focus on insulin secretion. J Clin Invest 2005;115:2047–58. [PubMed: 16075046]
7. Miki T, Seino S. Roles of K_{ATP} channels as metabolic sensors in acute metabolic changes. J Mol Cell Cardiol 2005;38:917–25. [PubMed: 15910876]
8. Nichols CG. K_{ATP} channels as molecular sensors of cellular metabolism. Nature 2006;440:470–6. [PubMed: 16554807]
9. Zingman LV, Alekseev AE, Bienengraeber M, Hodgson DM, Karger AB, Dzeja PP, Terzic A. Signaling in channel/enzyme multimers: ATPase transitions in SUR module gate ATP-sensitive K^+ conductance. Neuron 2001;31:233–45. [PubMed: 11502255]
10. Liu XK, Yamada S, Kane GC, Alekseev AE, Hodgson DM, O'Cochlain DF, Jahangir A, Miki T, Seino S, Terzic A. Genetic disruption of Kir6.2, the pore-forming subunit of ATP-sensitive K^+ channel, predisposes to catecholamine induced ventricular dysrhythmia. Diabetes 2004;53:S165–8. [PubMed: 15561906]

11. Selivanov VA, Alekseev AE, Hodgson DM, Dzeja PP, Terzic A. Nucleotide-gated K_{ATP} channels integrated with creatine and adenylate kinases: amplification, tuning and sensing of energetic signals in the compartmentalized cellular environment. Mol Cell Biochem 2004;256–7:243–56.
12. Gumina RJ, O'Cochlain DF, Kurtz CE, Bast PH, Pucar D, Mishra P, Miki T, Seino S, Macura S, Terzic A. K_{ATP} channel knockout worsens myocardial calcium stress load *in vivo* and impairs recovery in stunned heart. Am J Physiol Heart Circ Physiol 2007;292:H1706–13. [PubMed: 17189350]
13. Inagaki N, Gonoi T, Clement JP, Wang CZ, Aguilar-Bryan L, Bryan J, Seino S. A family of sulfonylurea receptors determines the pharmacological properties of ATP-sensitive K^+ channels. Neuron 1996;16:1011–7. [PubMed: 8630239]
14. Lorenz E, Terzic A. Physical association between recombinant cardiac ATP-sensitive K^+ channel subunits Kir6.2 and SUR2A. J Mol Cell Cardiol 1999;31:425–34. [PubMed: 10093054]
15. Zingman LV, Hodgson DM, Bienengraeber M, Karger AB, Kathmann EC, Alekseev AE, Terzic A. Tandem function of nucleotide binding domains confers competence to sulfonylurea receptor in gating ATP-sensitive K^+ channels. J Biol Chem 2002;277:14206–10. [PubMed: 11825892]
16. Park S, Lim BB, Perez-Terzic C, Mer G, Terzic A. Interaction of asymmetric *ABCC9*-encoded nucleotide binding domains determines K_{ATP} channel SUR2A catalytic activity. J Proteome Res 2008;7:1721–8. [PubMed: 18311911]
17. Zingman LV, Hodgson DM, Bast PH, Kane GC, Perez-Terzic C, Gumina RJ, Pucar D, Bienengraeber M, Dzeja PP, Miki T, Seino S, Alekseev AE, Terzic A. Kir6.2 is required for adaptation to stress. Proc Natl Acad Sci USA 2002;99:13278–83. [PubMed: 12271142]
18. Kane GC, Liu XK, Yamada S, Olson TM, Terzic A. Cardiac K_{ATP} channels in health and disease. J Mol Cell Cardiol 2005;38:937–43. [PubMed: 15910878]
19. Kane GC, Behfar A, Dyer RB, O'Cochlain DF, Liu XK, Hodgson DM, Reyes S, Miki T, Seino S, Terzic A. KCNJ11 gene knockout of the Kir6.2 K_{ATP} channel causes maladaptive remodeling and heart failure in hypertension. Hum Mol Genet 2006;15:2285–97. [PubMed: 16782803]
20. Kane GC, Lam CF, O'Cochlain DF, Hodgson DM, Reyes S, Liu XK, Miki T, Seino S, Katusic ZS, Terzic A. Gene knockout of the *KCNJ8*-encoded Kir6.1 K_{ATP} channel imparts fatal susceptibility to endotoxemia. FASEB J 2006;20:2271–80. [PubMed: 17077304]
21. Yamada S, Kane GC, Behfar A, Liu XK, Dyer RB, Faustino RS, Miki T, Seino S, Terzic A. Protection conferred by myocardial ATP-sensitive K^+ channels in pressure overload-induced congestive heart failure revealed in *KCNJ11* Kir6.2-null mutant. J Physiol 2006;577:1053–65. [PubMed: 17038430]
22. Bienengraeber M, Olson TM, Selivanov VA, Kathmann EC, O'Cochlain DF, Gao F, Karger AB, Ballew JD, Hodgson DM, Zingman LV, Pang YP, Alekseev AE, Terzic A. ABCC9 mutations identified in human dilated cardiomyopathy disrupt catalytic K_{ATP} channel gating. Nat Genet 2004;36:382–7. [PubMed: 15034580]
23. Olson TM, Alekseev AE, Moreau C, Liu XK, Zingman LV, Miki T, Seino S, Asirvatham SJ, Jahangir A, Terzic A. K_{ATP} channel mutation confers risk for vein of Marshall adrenergic atrial fibrillation. Nat Clin Pract Cardiovasc Med 2007;4:110–6. [PubMed: 17245405]
24. Reyes S, Terzic A, Mahoney DW, Redfield MM, Rodeheffer RJ, Olson TM. K_{ATP} channel polymorphism is associated with left ventricular size in hypertensive individuals: a large-scale community-based study. Hum Genet 2008;123:665–7. [PubMed: 18504616]
25. Drake TA, Ping P. Thematic review series: systems biology approaches to metabolic and cardiovascular disorders. Proteomics approaches to the systems biology of cardiovascular diseases. J Lipid Res 2007;48:1–8. [PubMed: 17065662]
26. Zlatkovic J, Arrell DK, Kane GC, Miki T, Seino S, Terzic A. Proteomic profiling of K_{ATP} channel-deficient hypertensive heart maps risk for maladaptive cardiomyopathic outcome. Proteomics 2009;9:1314–25. [PubMed: 19253285]
27. Hwang D, Lee IY, Yoo H, Gehlenborg N, Cho JH, Petritis B, Baxter D, Pitstick R, Young R, Spicer D, Price ND, Hohmann JG, Dearmond SJ, Carlson GA, Hood LE. A systems approach to prion disease. Mol Syst Biol 2009;5:252. [PubMed: 19308092]
28. Miki T, Nagashima K, Tashiro F, Kotake K, Yoshitomi H, Tamamoto A, Gonoi T, Iwanaga T, Miyazaki J, Seino S. Defective insulin secretion and enhanced insulin action in K_{ATP} channel-deficient mice. Proc Natl Acad Sci USA 1998;95:10402–6. [PubMed: 9724715]

29. Arrell DK, Elliott ST, Kane LA, Guo Y, Ko YH, Pedersen PL, Robinson J, Murata M, Murphy AM, Marbán E, Van Eyk JE. Proteomic analysis of pharmacological preconditioning. Novel protein targets converge to mitochondrial metabolism pathways. Circ Res 2006;99:706–14. [PubMed: 16946135]
30. Arrell DK, Niederländer NJ, Perez-Terzic C, Behfar A, Terzic A. Embryonic stem cell cardiac differentiation: a proteomic perspective. Adv Mol Med 2006;2:149–56.
31. Arrell DK, Neverova I, Fraser H, Marbán E, Van Eyk JE. Proteomic analysis of pharmacologically preconditioned cardiomyocytes reveals novel phosphorylation of myosin light chain 1. Circ Res 2001;89:480–7. [PubMed: 11557734]
32. Arrell DK, Niederländer N, Faustino RS, Behfar A, Terzic A. Cardioinductive network guiding stem cell differentiation revealed by proteomic cartography of TNFα-primed endodermal secretome. Stem Cells 2008;26:387–400. [PubMed: 17991915]
33. Arrell DK, Niederländer NJ, Perez-Terzic C, Behfar A, Terzic A. Pharmacoproteomics: advancing the efficacy and safety of regenerative therapeutics. Clin Pharmacol Ther 2007;82:316–9. [PubMed: 17671447]
34. Behfar A, Perez-Terzic C, Faustino RS, Arrell DK, Hodgson DM, Yamada S, Pucéat M, Niederländer N, Alekseev AE, Zingman LV, Terzic A. Cardiopoietic programming of embryonic stem cells for tumor-free heart repair. J Exp Med 2007;204:405–20. [PubMed: 17283208]
35. Link AJ, Eng J, Schieltz DM, Carmack E, Mize GJ, Morris DR, Garvik BM, Yates JR 3rd. Direct analysis of protein complexes using mass spectrometry. Nat Biotechnol 1999;17:676–82. [PubMed: 10404161]
36. Emanuelsson O, Nielsen H, Brunak S, von Heijne G. Predicting subcellular localization of proteins based on their N-terminal amino acid sequence. J Mol Biol 2000;300:1005–16. [PubMed: 10891285]
37. Shannon P, Markiel A, Ozier O, Baliga NS, Wang JT, Ramage D, Amin N, Schwikowski B, Ideker T. Cytoscape: a software environment for integrated models of biomolecular interaction networks. Genome Res 2003;13:2498–504. [PubMed: 14597658]
38. Assenov Y, Ramírez F, Schelhorn SE, Lengauer T, Albrecht M. Computing topological parameters of biological networks. Bioinformatics 2007;24:282–4. [PubMed: 18006545]
39. Barabási AL, Oltvai ZN. Network biology: understanding the cell's functional organization. Nat Rev Genet 2004;5:101–13. [PubMed: 14735121]
40. Anderson TW, Darling DA. Asymptotic theory of certain “goodness-of-fit” criteria based on stochastic processes. Ann Math Stat 1952;23:193–212.
41. Newman MEJ. The structure and function of complex networks. SIAM Rev 2003;45:167–256.
42. Maere S, Heymans K, Kuiper M. BiNGO: a Cytoscape plugin to assess overrepresentation of Gene Ontology categories in biological networks. Bioinformatics 2005;21:3448–9. [PubMed: 15972284]
43. Kane GC, Behfar A, Yamada S, Perez-Terzic C, O'Cochlain DF, Reyes S, Dzeja PP, Miki T, Seino S, Terzic A. ATP-sensitive K^+ channel knockout compromises the metabolic benefit of exercise training, resulting in cardiac deficits. Diabetes 2004;53:S169–75. [PubMed: 15561907]
44. Yamada S, Nelson TJ, Crespo-Diaz RJ, Perez-Terzic C, Liu XK, Miki T, Seino S, Behfar A, Terzic A. Embryonic stem cell therapy of heart failure in genetic cardiomyopathy. Stem Cells 2008;26:2644–53. [PubMed: 18669912]
45. Suzuki M, Li RA, Miki T, Uemura H, Sakamoto N, Ohmoto-Sekine Y, Tamagawa M, Ogura T, Seino S, Marbán E, Nakaya H. Functional roles of cardiac and vascular ATP-sensitive potassium channels clarified by Kir6.2-knockout mice. Circ Res 2001;88:570–7. [PubMed: 11282890]
46. Terzic A, Jahangir A, Kurachi Y. Cardiac ATP-sensitive K^+ channels: regulation by intracellular nucleotides and K^+ channel-opening drugs. Am J Physiol 1995;269:C525–45. [PubMed: 7573382]
47. Noma A. ATP-regulated K^+ channels in cardiac muscle. Nature 1983;305:147–8. [PubMed: 6310409]
48. Zingman LV, Alekseev AE, Hodgson-Zingman DM, Terzic A. ATP-sensitive potassium channels: metabolic sensing and cardioprotection. J Appl Physiol 2007;103:1888–93. [PubMed: 17641217]
49. Zingman LV, Hodgson DM, Alekseev AE, Terzic A. Stress without distress: homeostatic role for K_{ATP} channels. Mol Psychiatr 2003;8:253–4.
50. Carrasco AJ, Dzeja PP, Alekseev AE, Pucar D, Zingman LV, Abraham MR, Hodgson DM, Bienengraeber M, Pucéat M, Janssen E, Wieringa B, Terzic A. Adenylate kinase phosphotransfer communicates cellular energetic signals to ATP-sensitive potassium channels. Proc Natl Acad Sci USA 2001;98:7623–8. [PubMed: 11390963]

51. Crawford RM, Ranki HJ, Botting CH, Budas GR, Jovanoví A. Creatine kinase is physically associated with the cardiac ATP-sensitive K^+ channel *in vivo*. FASEB J 2002;16:102–4. [PubMed: 11729098]
52. Dhar-Chowdhury P, Harrell MD, Han SY, Jankowska D, Parachuru L, Morrissey A, Srivastava S, Liu W, Malester B, Yoshida H, Coetzee WA. The glycolytic enzymes, glyceraldehyde-3-phosphate dehydrogenase, triose-phosphate isomerase, and pyruvate kinase are components of the K_{ATP} channel macromolecular complex and regulate its function. J Biol Chem 2005;280:38464–70. [PubMed: 16170200]
53. Jovanović S, Du Q, Crawford RM, Budas GR, Stagljar I, Jovanović A. Glyceraldehyde 3-phosphate dehydrogenase serves as an accessory protein of the cardiac sarcolemmal K_{ATP} channel. EMBO Rep 2005;6:848–52. [PubMed: 16082386]
54. Liu GX, Hanley PJ, Ray J, Daut J. Long-chain acyl-coenzyme A esters and fatty acids directly link metabolism to K_{ATP} channels in the heart. Circ Res 2001;88:918–24. [PubMed: 11349001]
55. Abraham MR, Selivanov VA, Hodgson DM, Pucar D, Zingman LV, Wieringa B, Dzeja PP, Alekseev AE, Terzic A. Coupling of cell energetics with membrane metabolic sensing: Integrative signaling through creatine kinase phosphotransfer disrupted by M-CK gene knock-out. J Biol Chem 2002;277:24427–34. [PubMed: 11967264]
56. Crawford RM, Budas GR, Jovanović S, Ranki HJ, Wilson TJ, Davies AM, Jovanović A. M-LDH serves as a sarcolemmal K_{ATP} channel subunit essential for cell protection against ischemia. EMBO J 2002;21:3936–48. [PubMed: 12145195]
57. Albert R, Jeong H, Barabási AL. Error and attack tolerance of complex networks. Nature 2000;406:378–82. [PubMed: 10935628]
58. Loscalzo J, Kohane I, Barabási AL. Human disease classification in the postgenomic era: a complex systems approach to human pathobiology. Mol Syst Biol 2007;3:124. [PubMed: 17625512]
59. Meng C, Jin X, Xia L, Shen SM, Wang XL, Cai J, Chen GQ, Wang LS, Fang NY. Alterations of mitochondrial enzymes contribute to cardiac hypertrophy before hypertension development in spontaneously hypertensive rats. J Proteome Res 2009;8:2463–75. [PubMed: 19265432]
60. Sutak R, Xu X, Whitnall M, Kashem MA, Vyoral D, Richardson DR. Proteomic analysis of hearts from frataxin knockout mice: marked rearrangement of energy metabolism, a response to cellular stress and altered expression of proteins involved in cell structure, motility and metabolism. Proteomics 2008;8:1731–41. [PubMed: 18340635]
61. Hodgson DM, Zingman LV, Kane GC, Perez-Terzic C, Bienengraeber M, Ozcan C, Gumina RJ, Pucar D, O'Coclain DF, Mann DL, Alekseev AE, Terzic A. Cellular remodeling in heart failure disrupts K_{ATP} channel-dependent stress tolerance. EMBO J 2003;22:1732–42. [PubMed: 12682006]
62. Gumina RJ, Pucar D, Bast PH, Hodgson DM, Kurtz CE, Dzeja PP, Miki T, Seino S, Terzic A. Knockout of Kir6.2 negates ischemic preconditioning-induced protection of myocardial energetics. Am J Physiol Heart Circ Physiol 2003;284:H2106–13. [PubMed: 12598229]
63. Terzic A, Tung RT, Kurachi Y. Nucleotide regulation of ATP-sensitive potassium channels. Cardiovasc Res 1994;28:746–53. [PubMed: 7923274]
64. Jahangir A, Terzic A. K_{ATP} channel therapeutics at the bedside. J Mol Cell Cardiol 2005;39:99–112. [PubMed: 15953614]
65. Sattiraju S, Reyes S, Kane GC, Terzic A. K_{ATP} channel pharmacogenomics: from bench to bedside. Clin Pharmacol Ther 2008;83:354–7. [PubMed: 17957187]
66. Chen CH, Budas GR, Churchill EN, Disatnik MH, Hurley TD, Mochly-Rosen D. Activation of aldehyde dehydrogenase-2 reduces ischemic damage to the heart. Science 2008;321:1493–5. [PubMed: 18787169]
67. Ping P. Getting to the heart of proteomics. N Engl J Med 2009;360:532–4. [PubMed: 19179323]
68. Mayr M, Chung YL, Mayr U, McGregor E, Troy H, Baier G, Leitges M, Dunn MJ, Griffiths JR, Xu Q. Loss of PKC-delta alters cardiac metabolism. Am J Physiol Heart Circ Physiol 2004;287:H937–45. [PubMed: 15277208]
69. Mayr M, Metzler B, Chung YL, McGregor E, Mayr U, Troy H, Hu Y, Leitges M, Pachinger O, Griffiths JR, Dunn MJ, Xu Q. Ischemic preconditioning exaggerates cardiac damage in PKC-delta null mice. Am J Physiol Heart Circ Physiol 2004;287:H946–56. [PubMed: 15277209]
70. Mayr M, Liem D, Zhang J, Li X, Avliyakulov NK, Yang JI, Young G, Vondriska TM, Ladroue C, Madhu B, Griffiths JR, Gomes A, Xu Q, Ping P. Proteomic and metabolomic analysis of

cardioprotection: Interplay between protein kinase C epsilon and delta in regulating glucose metabolism of murine hearts. J Mol Cell Cardiol 2009;46:268–77. [PubMed: 19027023]

71. Dzeja PP, Redfield MM, Burnett JC, Terzic A. Failing energetics in failing hearts. Curr Cardiol Rep 2000;2:212–7. [PubMed: 10980895]
72. Terzic A, Moore RL, Waldman SA. Acquired and innate cardioprotection. J Appl Physiol 2007;103:1436–7. [PubMed: 17690193]
73. Ingwall JS. Energy metabolism in heart failure and remodelling. Cardiovasc Res 2009;81:412–9. [PubMed: 18987051]

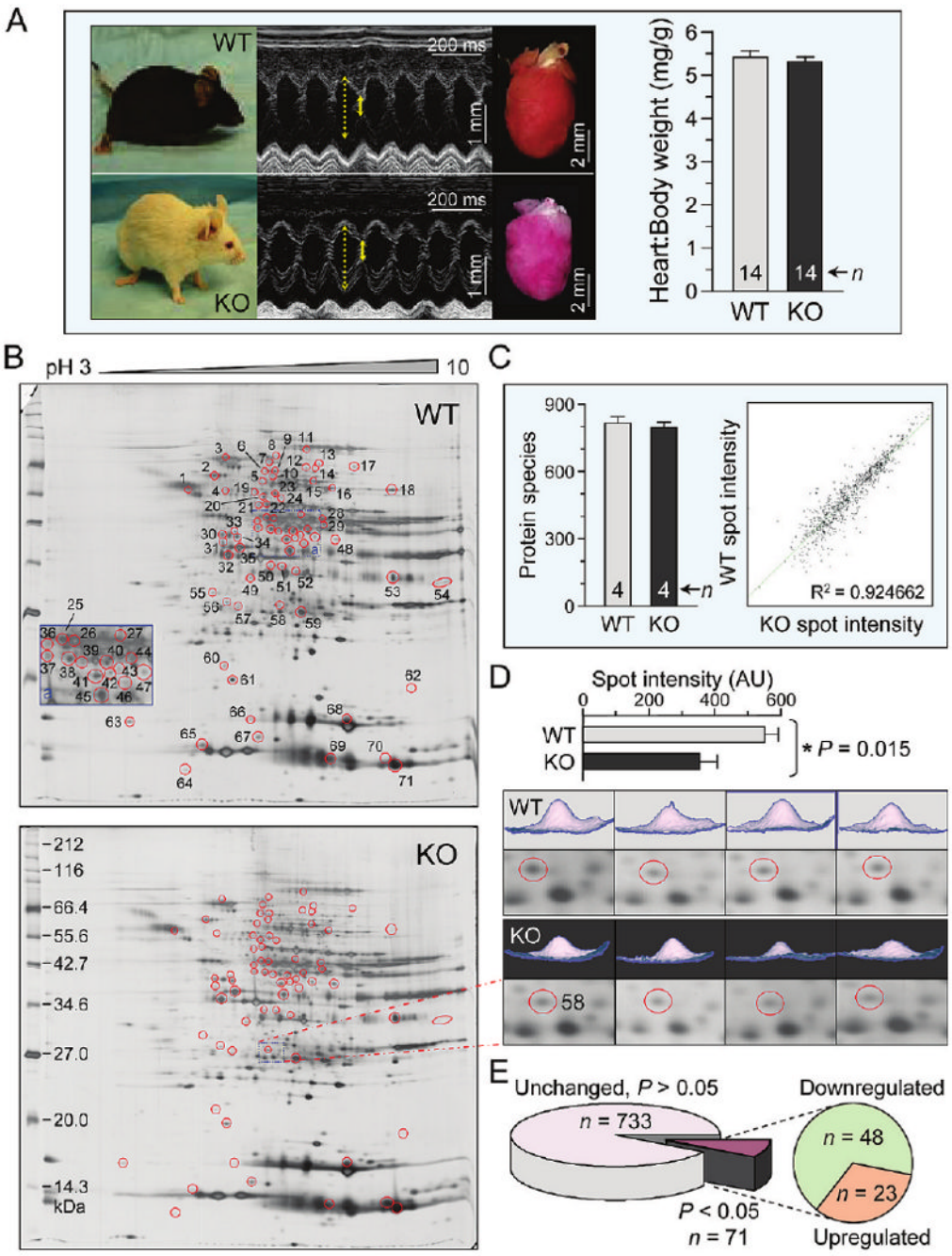

Figure 1.

Kir6.2 deletion remodels the ventricular proteome. (A) Adult age and sex-matched wild-type (WT) and Kir6.2-knockout (KO) mice assessed under stress-free conditions by ventricular M-mode echocardiography exhibited no apparent differences in function (solid and dotted yellow lines indicate extent of systolic and diastolic wall motion, respectively), nor were there differences in gross heart morphology or heart to body weight ratio. (B) Silver-stained 2-D gels of left ventricular cytoplasmic protein extracts (100 μg per gel) from WT and KO mice resolved by pH 3–10 IEF, 12.5% SDS-PAGE. Differentially expressed spots are circled and numbered to cross-reference with corresponding protein assignments determined by LTQ-Orbitrap MS/MS analysis of excised tryptic digests. (C) Gel reproducibility was demonstrated

by consistent numbers of detected protein species and strong correlation ($R^2 = 0.925$) across treatments between average normalized intensities of matching protein spots from WT and KO gels. (D) Example of spot quantification (top), indicating 2-D gel position and 3-D rendering of the quantified spot from all resolved gels (bottom, $n = 4$ for WT and KO). (E) Densitometric analysis comparing WT to KO revealed that 71 of 804 spots differed ($P < 0.05$), including 23 up-regulated and 48 down-regulated protein species.

Protein Name (Node Symbol) Spot Number(s)	Swiss-Prot Accession	Mascot Score	Unique Peptides	Sequence Cov. (%)	Predicted Mr	Predicted pI	Fold Change		
3-hydroxyisobutyrate dehydrogenase (Hibadh) **49**	Q99L13	248	5	25.7	31742	6.01	-1.61	Mitochondrial	Metabolism
3-oxoacyl-[acyl-carrier-protein] synthase (Oxsm) **21**	Q9D404	55	1	3.0	45523	6.29	-2.64		
Acetyl-CoA acetyltransferase (Acat1) **29**	Q8QZT1	224	4	19.8	41414	8.18	8.58		
Acetyl-coenzyme A synthetase 2-like (Acss1) **8**	Q99NB1	44	1	1.7	70724	5.98	1.70		
Aconitate hydratase (Aco2) **11**, 12, 14, 15	Q99KI0	354	8	11.5	82464	7.40	2.10		
Acyl-coenzyme A thioesterase 2 (Acot2) **25**, **26**, 38	Q9QYR9	644	11	25.6	44934	6.14	-1.44		
Creatine kinase, sarcomeric (Ckmt2) **29**	Q6P8J7	41	1	3.3	43387	7.72	8.58		
Dihydrolipoyllysine-residue acetyltransferase (Dlat) **12**	Q8BMF4	37	1	3.2	58778	5.70	-1.59		
Dihydrolipoyllysine-residue succinyltransferase (Dlst) **19**, **20**	Q9D2G2	167	3	7.7	41470	5.98	-1.61		
Electron transfer flavoprotein subunit α (Etfa) **50**, **52**	Q99LC5	102	2	9.9	32767 ‡	6.93 ‡	-1.64		
Electron transfer flavoprotein subunit β (Etfb) **58**	Q9DCW4	38	1	3.9	27623	8.25	-1.56		
Enoyl-CoA hydratase (Echs1) **58**	Q8BH95	287	6	31.2	28475	7.78	-1.56		
Fumarate hydratase (Fh) **29**, 21	P97807	72	1	3.9	49935	7.88	8.58		
Hydroxyacyl-coenzyme A dehydrogenase (Hadh) **53**	Q61425	362	9	34.8	32995	8.26	2.22		
Isocitrate dehydrogenase [NAD] subunit α (Idh3a) **30**, **33**, **34**	Q9D6R2	748	14	39.6	36707	5.60	-1.53		
Isocitrate dehydrogenase 3, NAD+, β (Idh3b) **38**, **41**	Q91VA7*	85	2	5.2	42195	8.76	-1.69		
Lipoamide acyltransferase (Dbt) **20**	P53395	619	14	24.9	46188	6.17	-1.55		
Long-chain specific acyl-CoA dehydrogenase (Acadl) 24, **25**, **26**, 38, 41	P51174	409	6	17.2	44627	6.50	-1.44		
Malate dehydrogenase (Mdh2) **54**	P08249	511	10	38.5	33139	8.55	-152		
Medium-chain specific acyl-CoA dehydrogenase (Acadm) **29**	P45952	52	1	3.1	43593	7.69	8.58		
Methylmalonate-semialdehyde dehydrogenase (Aldh6a1) **16**	Q9EQ20*	769	13	31.1	47556 ‡	7.71 ‡	1.42		
Pyruvate dehydrogenase E1 α (Pdha1) **21**, **26**	P35486	124	3	8.0	40181	6.78	-1.60		
Pyruvate dehydrogenase E1 β (Pdhb) **32**	Q9D051	478	9	33.4	35768	5.39	1.52		
Pyruvate dehydrogenase protein X (Pdhx) **19**	Q8BKZ9	118	3	5.6	47948	5.82	-1.74		
Short/branched chain acyl-CoA dehydrogenase (Acadsb) **38**	Q9DBL1	282	5	14.6	44041	6.06	-1.66		
Short-chain specific acyl-CoA dehydrogenase (Acads) **37**, **38**, **41**	Q07417	500	9	28.6	42231	7.12	-1.67		
Succinate dehydrogenase flavoprotein subunit (Sdha) **7**	Q8K2B3	505	9	20.5	68032	6.32	-1.55		
Succinate semialdehyde dehydrogenase (Aldh5a1) **24**	Q8BWF0	148	4	8.6	52012	7.12	-1.63		
Succinyl-CoA:3-ketoacid-coA transferase 1 (Oxct1) **16**	Q9D0K2	1070	17	46.5	51877	7.01	1.42		
6-phosphogluconolactonase (Pgls) **56**	Q9CQ60	290	6	31.5	27254	5.55	-2.33	Cytoplasmic	
Acyl-coenzyme A thioesterase 1 (Acot1) **32**, **34** (and/or Acot2)	O55137	266	4	15.0	46136	6.12	-1.74		
α-enolase (Eno1) **22**	P17182	376	6	19.4	47010	6.36	-2.86		
Aldose 1-epimerase (Galm) **40**	Q8K157	29	1	4.4	37799	6.26	-1.21		
β-enolase (Eno3) **21**, **22**	P21550	495	8	24.0	46894	6.81	-2.79		
Creatine kinase M-type (Ckm) **26**	P07310	81	1	3.7	43045	6.58	-1.52		
Fructose-bisphosphate aldolase A (Aldoa) **29**	P05064	318	5	23.6	39225	8.40	8.58		
Glucose-6-phosphate isomerase (Gpi) **16**, **18**	P06745**	578	10	24.7	62636	8.18	-6.35 1.42		
Glyceraldehyde-3-phosphate dehydrogenase (Gapdh) **54**	P16858	37	1	4.2	35679	8.45	-152		
L-lactate dehydrogenase B chain (Ldhb) 30, 34, **35**, 41, 43, 51, 64	P16125	849	15	37.2	36441	5.70	1.38		
Malate dehydrogenase (Mdh1) 19, 21, **32**, 34, 35, 36	P14152	122	3	10.5	36780	6.16	1.52		
Nucleoside diphosphate-linked moiety X motif 8 (Nudt8) **58**	Q9CR24 †	128	3	21.5	20540 ‡	6.06 ‡	-1.56		
Phosphofructokinase 1 (Pfkm) **11**	P47857	56	1	2.2	85137	8.23	2.10		
Phosphoglucomutase-1 (Pgm1) **6**, **9**	Q9D0F9	1562	27	64.4	61386	6.32	-1.61		
Pyruvate kinase isozymes M1/M2 (Pkm2) 11, **15**	P52480	1543	26	52.9	57714	7.42	1.49		
Sorbitol dehydrogenase (Sord) **41**	Q64442	489	10	31.7	38249	6.56	-1.73		
Triosephosphate isomerase (Tpi1) **59**	P17751	367	6	25.0	26581	7.09	1.28		
3-hydroxyisobutyryl-CoA hydrolase (Hibch) 15, 34, **40**	Q8QZS1	419	8	20.0	39239	6.24	-1.21	Amino Acid	
Alanine aminotransferase 1 (Gpt) **19**	Q8QZR5	271	6	12.1	55011	6.26	-1.74		
Aspartate aminotransferase (Got2) **29**	P05202	59	1	3.3	44579	8.97	8.58		
Branched-chain-amino-acid aminotransferase (Bcat2) **43**, **47**, **48**	O35855	323	7	20.8	41176	7.70	2.11		
ES1 protein homolog (C21orf33) **59**	Q9D172	56	1	6.6	23920	7.31	1.28		
Fumarylacetoacetase (Fah) **29**	P35505	424	8	31.7	46104	6.92	8.58		
Fumarylacetoacetate hydrolase domain-containing protein 2A (Fahd2a) **50**, **51**	Q3TC72 †	62	1	5.4	34690	8.42	-1.45		
Isovaleryl-CoA dehydrogenase (Ivd) **36**, **38**	Q9JHI5	327	7	19.3	42971	6.29	-1.65		
Methionine adenosyltransferase 2 (Mat2a) **20**	Q3THS6	72	1	3.3	43689	6.02	-1.55		
Methylcrotonoyl-CoA carboxylase β chain (Mccc2) **15**	Q3ULD5	311	6	14.2	52383 ‡	6.13 ‡	1.49		
ADP-ribosylhydrolase 2 (Adprhl1) 17, **33**	Q8BGK2 †	330	6	21.8	39885	5.62	-1.32	Nucleic Acid	
Bifunctional purine biosynthesis protein PURH (Atic) **6**, **9**	Q9CWJ9	399	8	18.2	64217	6.30	-1.61		
Carboxylesterase 3 (Ces1) **5**	Q8VCT4	92	2	4.0	59839	6.18	-4.40		
Cytosolic 5'-nucleotidase III (Nt5c3) **32**	Q9D020	71	1	3.9	37252	6.21	1.52		
Glycosyltransferase 8 domain-containing protein 3 (Glt8d3) **35**	Q3UHH8 †	38	1	2.0	46491	9.14	1.38		
Guanosine monophosphate reductase 1 (Gmpr) **42**	Q9DCZ1	52	2	6.1	37482	6.64	-2.01		
Trifunctional purine biosynthetic protein adenosine-3 (Gart) **19**	Q64737	31	1	0.8	107395	6.25	-1.74		

Figure 2.

Metabolic remodeling is the primary effect of K_{ATP} channel deficiency. Proteins assigned by LTQ-Orbitrap MS/MS analysis from significantly altered spots were functionally categorized by Swiss-Prot ontological annotations. The primary association was with metabolic processes, as 63/102 protein assignments encompassed mitochondrial, cytoplasmic, and amino or nucleic acid metabolic functions. Protein names are listed with their Swiss-Prot gene name (for Node Symbol) to locate them in the protein interaction network, and with their corresponding spot numbers from their 2-D gel positions. Protein accession number, Mascot score, number of unique identified peptides, % sequence cov. (coverage), predicted M_r and p*I* for each protein (following expected post-translational processing, e.g., removal of a known or predicted

mitochondrial signal peptide), and fold change (KO versus WT) are indicated. For proteins detected in more than one spot, maximum score and number of unique peptides are reported. Fold change was calculated as described in experimental procedures, and for proteins detected in both increasing and decreasing spots (**), both values are indicated. Complete MS/MS data for all proteins is outlined in Supplementary Table 1 (Supporting Information). (*TrEMBL entry; ** Contains both up- and down-regulated spots; † Node not detected for network analysis by Ingenuity Pathways; ‡ M_r/p*I* calculated after TargetP 1.1 prediction of mitochondrial localization and signal peptide cleavage site).

Protein Name (Node Symbol) Spot Number(s)	Swiss-Prot Accession	Mascot Score	Unique Peptides	Sequence Cov. (%)	Predicted Mr	Predicted pI	Fold Change	
Aflatoxin B1 aldehyde reductase 2 (Akr7a2) **40**	Q8CG76	67	1	3.3	40598	8.36	-1.21	Oxidoreductase
Alcohol dehydrogenase class 3 (Adh5) **41**	P28474	401	8	27.3	39417	7.11	-1.73	
Aldehyde dehydrogenase (Aldh2) **19**, **20**, **23**	P47738	829	15	34.3	54375	6.05	-1.51	
Aldose reductase (Akr1b1) **45**	P45376	62	1	4.4	35601	6.79	-1.24	
Catalase (Cat) **15**	P24270	460	9	20.7	59634	7.72	1.49	
Glutathione S-transferase μ 1 (Gstm1) **58**, **59**	P10649 **	141	2	9.7	25839	8.14	-1.56 1.28	
Peroxiredoxin-5 (Prdx5) **68**	P99029	37	1	6.8	17015	7.70	1.62	
Thioredoxin reductase 2 (Txnrd2) **16**	Q9JLT4	58	1	2.3	52990	7.08	1.42	
Actin-related protein 2/3 complex subunit 4 (Arpc4) **62**	P59999	271	6	34.1	19536	8.53	-3.59	Cytostructure/ Scaffolding
Adenylyl cyclase-associated protein 1 (Cap1) **16**	P40124	288	6	14.4	51444	7.30	1.42	
Chloride intracellular channel protein 4 (Clic4) **55**	Q9QYB1	115	2	9.5	28598	5.45	-6.38	
Dynamin-related protein 1 (Dnm1l) **8**	Q8K1M6	142	3	4.3	82658	6.61	1.70	
Moesin (Msn) **8**	P26041	1348	27	44.8	67636	6.24	1.70	
Myoglobin (Mb) 3, 8, 12, 14, **68**	P04247	426	9	64.1	16938	7.23	1.62	
Tubulin β-2C (Tubb2c) **1**	P68372	238	5	13.3	49831	4.79	2.40	
WD repeat protein 1 (Wdr1) **7**	O88342	569	12	21.6	66276	6.12	-1.55	
60 kDa heat shock protein (Hspd1) **2**	P63038	638	12	23.9	57926	5.35	-2.31	Chaperone
Heat shock 70 kDa protein 8 (Hspa8) **3**	P63017	58	1	1.7	70871	5.37	2.03	
Heat shock 70 kDa protein 9 (Hspa9) **3**	P38647	1708	27	51.8	68613	5.50	2.03	
Heat-shock protein β-1 (Hspb1) **57**	P14602	196	4	34.9	23014	6.12	-6.92	
Heat-shock protein β-6 (Hspb6) **61**	Q5EBG6	188	4	38.3	17521	5.64	-1.76	
T-complex protein 1 subunit ζ (Cct6a) **6**, **9**	P80317	62	1	3.2	57873	6.67	-1.61	
26S protease regulatory subunit S10B (Psmc6) **29**	P62334	378	6	20.6	44042	7.25	8.58	Protein Catabolism
26S proteasome non-ATPase regulatory subunit 11 (Psmd11) **21**, **22**	Q8BG32	233	5	13.1	47306	6.09	-2.79	
26S proteasome non-ATPase regulatory subunit 7 (Psmd7) **40**	P26516	132	3	9.0	36409	6.31	-1.21	
Proteasome subunit α 3 (Psma3) **55**	O70435	520	10	38.2	28274	5.29	-6.38	
Proteasome subunit α 6 (Psma6) **58**	Q9QUM9	688	11	45.1	27372	6.35	-1.56	
Putative ATP-dependent Clp protease proteolytic subunit (Clpp) **56**	O88696	64	2	10.0	24248 ‡	5.55 ‡	-2.33	
14-3-3 ε (Ywhae) **64**	P62259	65	1	5.1	29174	4.63	-2.79	Signaling Regulation
Annexin A3 (Anxa3) **32**	O35639	108	3	10.2	36240	5.33	1.52	
Dihydropyrimidinase-related protein 2 (Dpysl2) **6**, **9**	O08553	375	6	14.2	62278	5.95	-1.61	
Mitogen-activated protein kinase 1, ERK-2 (Mapk1) **41**	P63085	86	2	5.9	41144	6.53	-1.73	
Sarcalumenin (Srl) **19**	Q7TQ48 †	166	3	4.1	97093	4.38	-1.74	
Serine/threonine-protein phosphatase PP1-β (Ppp1cb) **35**	P62141	62	1	3.1	37056	5.85	1.38	
39S ribosomal protein L12 (Mrpl12) **60**	Q9DB15	241	5	29.0	16653	5.39	-2.27	Transcription/ Translation
Elongation factor 1-gamma (Eef1g) **22**	Q9D8N0	148	3	7.6	49930	6.33	-2.86	
Eukaryotic translation initiation factor 3 subunit γ (Eif3h) **39**	Q91WK2	47	1	5.4	39832	6.19	-2.96	
Heterogeneous nuclear ribonucleoprotein A/B (Hnrpab) **40**	Q99020	39	1	4.9	30831	7.69	-1.21	
Heterogeneous nuclear ribonucleoprotein H (Hnrph1) AND/OR hnRNP H' (Hnrph2) **26**	O35737 P70333	41	1	3.8 3.8	49068 49280	5.89 5.89	-1.52	

Figure 3.

Secondary functions associated with K_{ATP} channel deficiency form an infrastructure supporting metabolism. Ontological categorization indicated that a secondary functional group consisting of the remaining identified proteins (39/102) comprises a number of functions supporting cellular metabolic activity. These proteins function as oxidoreductases, in cytostructure and scaffolding, as stress-related chaperones, or in protein catabolism, signaling regulation, or transcription and translation. Protein names are listed with their Swiss-Prot gene name (for Node Symbol) to locate them in the protein interaction network, and with their corresponding spot numbers from their 2-D gel positions. Protein accession number, Mascot score, number of unique identified peptides, % sequence cov. (coverage), predicted M_r and p*I* for each protein (following expected post-translational processing, for example, removal of a mitochondrial signal peptide), and fold change (KO versus WT) are indicated. For proteins detected in more than one spot, maximum score and number of unique peptides are reported. Fold change was calculated as described in experimental procedures, and for proteins detected in both increasing and decreasing spots (**), both values are indicated. Complete MS/MS data for all proteins is outlined in Supplementary Table 1 (Supporting Information). (**Contains both up- and down-regulated spots; † Node not detected for network analysis by Ingenuity Pathways; ‡ M_r/p*I* calculated after TargetP 1.1 prediction of mitochondrial localization and signal peptide cleavage site).

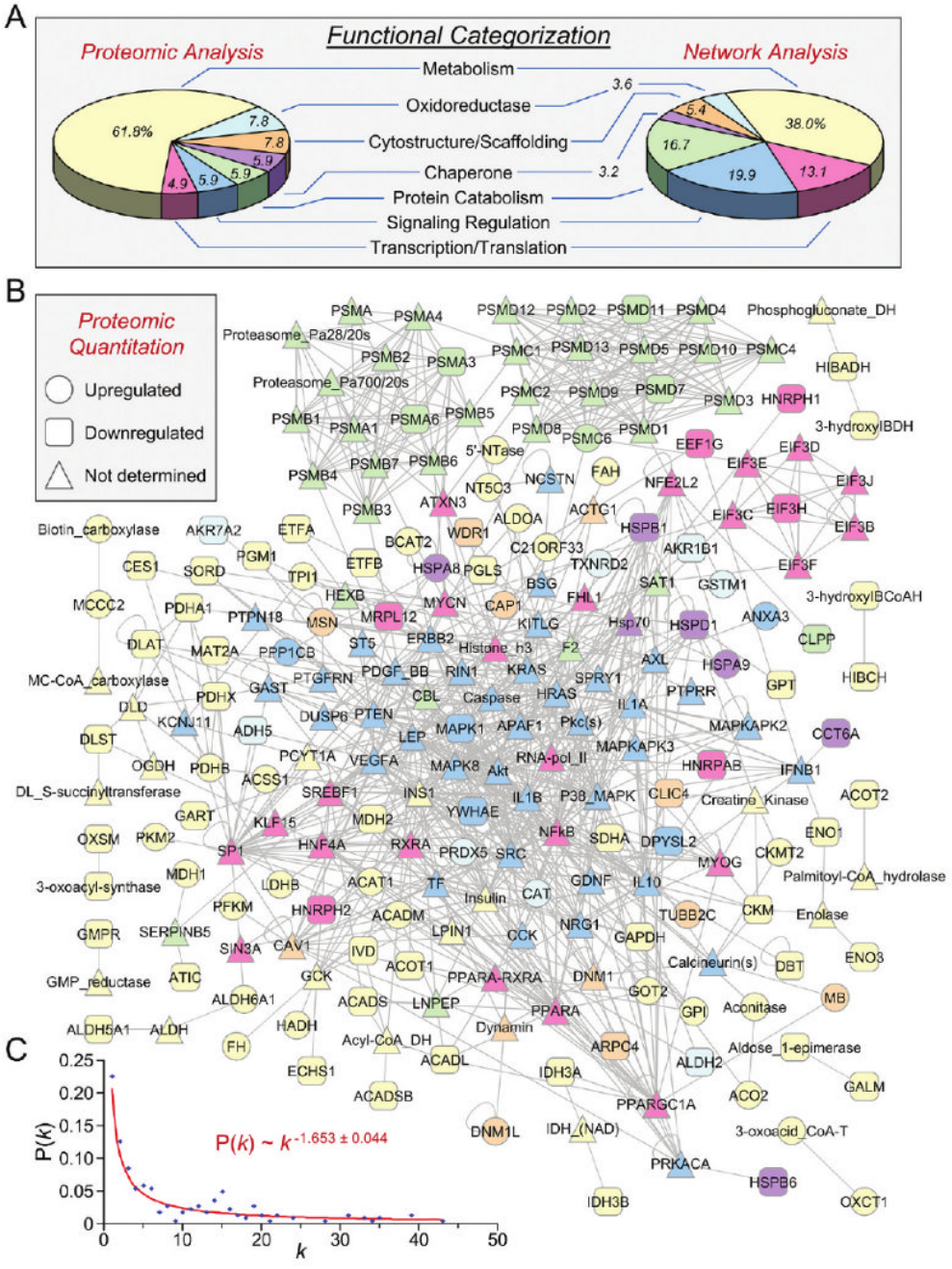

Figure 4.

Network analysis of the Kir6.2-dependent proteome. (A) The distribution of Swiss-Prot annotated primary ontological functions of altered proteins (Proteomic Analysis) carry through to the expanded protein interaction network (Network Analysis), with metabolism predominant in both. (B) Differentially expressed proteins of the Kir6.2-dependent subproteome submitted to Ingenuity Pathways Analysis as focus nodes generated a 221 protein interaction network. Nodes are listed by Swiss-Prot gene designations, with the exception of nodes representing protein families. Node color corresponds to ontological function (from A), while node shape (legend) indicates directionality of expression level change for proteins characterized during proteomic analysis. (C) Network degree distribution, (P[*k*]) versus degree (*k*), followed a power

law distribution indicating nonstochastic scale-free network architecture characteristic of biological networks.

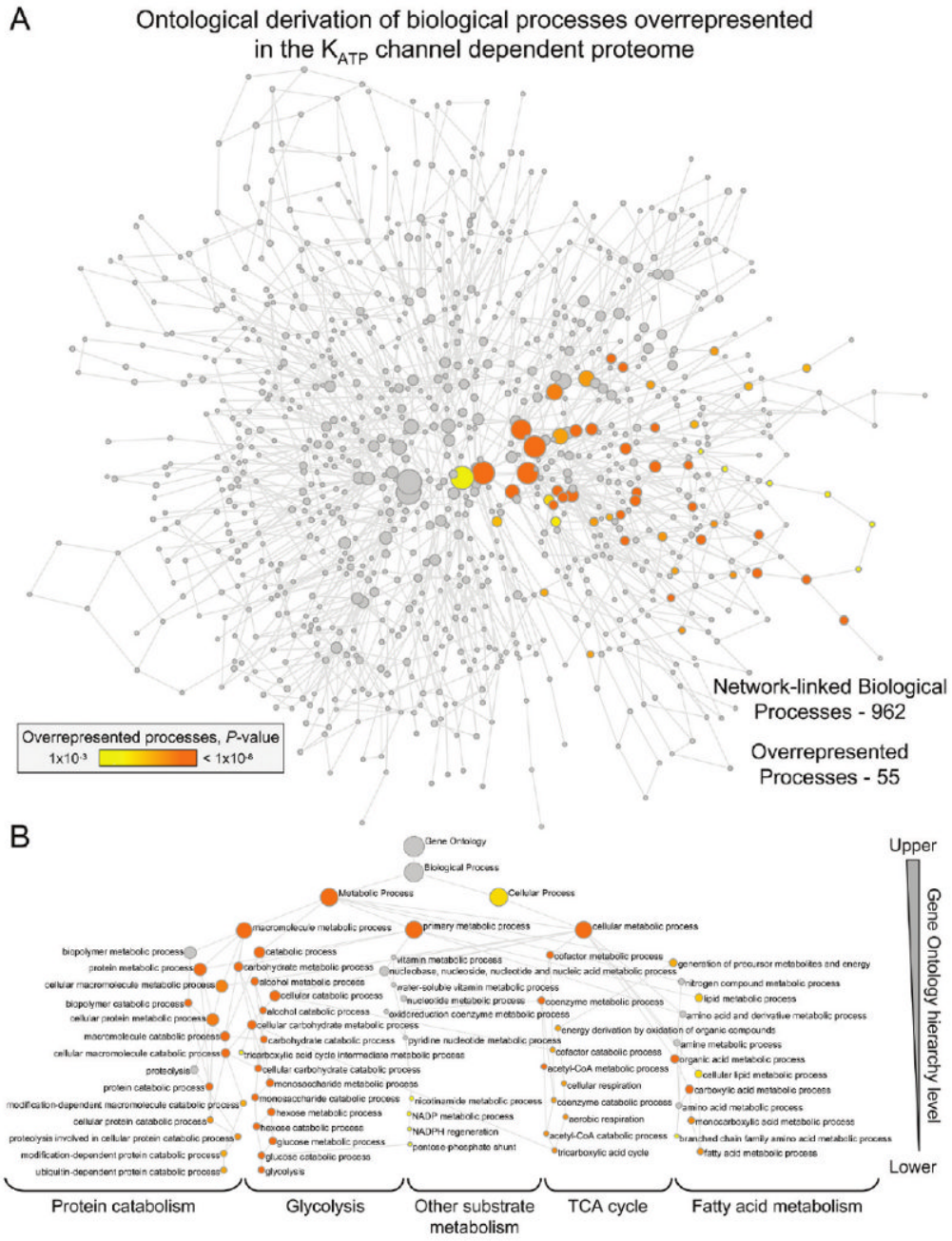

Figure 5.

Biological processes linked to the K_{ATP} channel-dependent protein interaction network. (A) K_{ATP} channel-dependent protein interaction network was interrogated with the Cytoscape module BiNGO to identify network-linked Gene Ontology (GO) biological processes, including evidence of overrepresentation. The derived GO network consisted of 962 processes (nodes), of which 55 were significantly overrepresented (colored nodes, $P < 0.001$), with nodes connected by GO hierarchical relationships. Node size is proportional to the number of network proteins annotated to that biological process, while node shading represents a 5-log gradient of significant, false discovery rate-corrected *P*-values, with gray nodes not significantly overrepresented. (B) Hierarchical layout of overrepresented biological processes from panel

A, with node size/color retained and identities indicated. Of note, all 55 colored nodes involve metabolic processes. Functional interdependencies within the GO hierarchy translated into significant overrepresentation by entire hierarchical branches, with the most significant nodes furthest down the hierarchy offering the strongest interpretive explanation. Processes linked to “Glycolysis”, the “TCA cycle”, “Fatty acid metabolism” and “Protein catabolism” demonstrated the greatest overrepresentation.

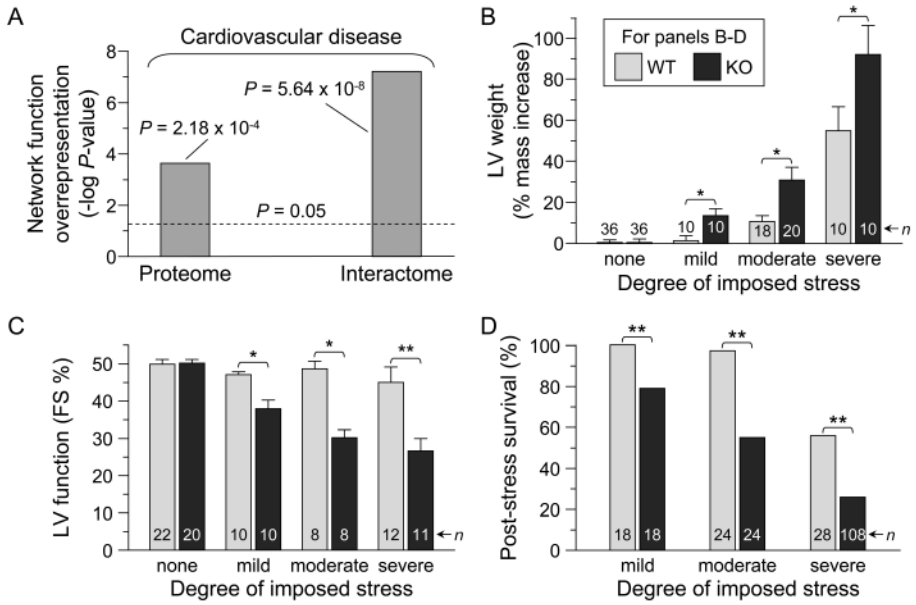

Figure 6.

Predicted outcome of K_{ATP} channel deficit and functional validation. (A) "Cardiovascular disease" was significantly overrepresented as a consequence of K_{ATP} channel deficit based on Ingenuity Pathways Analysis of both the K_{ATP} channel-dependent altered proteins (Proteome) and their derived protein network (Interactome). (B–D) Functional confirmation of predicted outcome. While wild-type (WT) and Kir6.2-knockout (KO) counterparts exhibited no difference in structural or functional parameters in the absence of imposed stress, progressively greater challenge by mild (chronic repetitive aquatic exercise), moderate (deoxycorticosterone acetate/salt-induced hypertension) or severe (transverse aortic constriction) stress led to aggravated increases in left ventricular (LV) mass (B; $*P < 0.05$) and decreases in LV fractional shortening, FS (C; $*P < 0.05$, $**P < 0.01$), with K_{ATP} channel deletion ultimately leading to decreasing post-stress survival (D; $**P < 0.01$ versus WT).